

Porous cordierite-supported polyethyleneimine composites for nickel(II) and cadmium(II) ions removal

Nina Obradović^a, Jelena Rusmirović^{b,c,*}, Suzana Filipović^a, Darko Kosanović^a, Aleksandar Marinković^d, Danka Radić^e, Vladimir Pavlović^{a,e}

^aInstitute of Technical Sciences of SASA, 11000 Belgrade, Serbia

^bMilitary Technical Institute, Ratka Resanovića 1, 11000 Belgrade, Serbia, email: jrusmirovic@tmf.bg.ac.rs (J. Rusmirović)

^cInnovation center, Faculty of Technology and Metallurgy, University of Belgrade, 11120 Belgrade, Serbia

^dFaculty of Technology and Metallurgy, University of Belgrade, 11120 Belgrade, Serbia

^eFaculty of Agriculture, University of Belgrade, 11000 Belgrade, Serbia

Received 25 September 2019; Accepted 21 February 2020

ABSTRACT

Industrial/technological growth is directly connected with environmental pollution, but its influence can be minimized through pollution abatement approaches such as the treatment of industrial wastewater. In this study, novel porous amine-functionalized silicate minerals, specifically, cordierite was investigated for the removal of toxic heavy metals from industrial wastewaters. Cordierite supports were synthesized by mixing MgO, Al₂O₃ and SiO₂ powders in 2:2:5 molar ratios, and mechanically activated via ball milling in ethanol for 10, 40, or 80 min. Pellets were sintered by heating in air at 20°C min⁻¹ to 1,350°C, for 2 h. Porous supports were produced by coarsely crushing the sintered pellets and mixing the crushed and sieved cordierite powder with 20 wt.% of a pore-forming agent, either nanocellulose or yeast. The resulting pellets were sintered by heating at 5°C min⁻¹ to 700°C in air. The synthetic cordierite support was modified by treatment in polyethyleneimine. Activated supports were then tested for the removal of Ni²⁺ and Cd²⁺ ions. The phase composition of the cordierite supports was analyzed by the X-ray diffraction, Fourier-transform infrared spectroscopy, and scanning electron microscopy. Analysis of adsorption isotherms, kinetics, and thermodynamic parameters indicated that adsorption was a spontaneous, endothermic process with a maximum adsorption capacity of 36 mg g⁻¹ for Cd²⁺ and 43 mg g⁻¹ for Ni²⁺. This work has shed light on the mechanism of heavy metal removal from the aquatic medium using the novel hybrid functionalized cordierite-based ceramic.

Keywords: Adsorption capacity; Cordierite; Heavy metals; Porous ceramics; Sorbent

1. Introduction

Intensive industrial development has increased the amount of chemical waste in effluents. Examples include volatile industrial reagents, heavy metals in ionic form, and pharmaceuticals, etc. [1–3]. Chemical wastes are a

primary environmental hazard and they deteriorate water quality [1,4]. Cadmium and nickel in ionic form (Cd²⁺ and Ni²⁺) are among the toxic metals that are released into the environment. They are more mobile than other metals and represent serious threats to human health. Industrial and agricultural activities such as mining, smelting, fertilizer

* Corresponding author.

production, and processing of sewage sludge lead to Cd^{2+} and Ni^{2+} pollution worldwide [5]. Moreover, Cd^{2+} and Ni^{2+} are present in oils, pneumatics, and old cars [6]. The U.S. Environmental Protection Agency (EPA) limits the concentration of Cd^{2+} to 0.005 ppm, and of Ni^{2+} to 0.1 ppm in water [7]. Numerous treatment technologies for ionic forms of heavy metals have been developed to mitigate the uncontrolled emissions of these harmful metals in surface water [8]. Among them, solvent extraction, chemical precipitation, evaporation, electrochemical treatment, membrane filtration, and emerging metal-organic frameworks are high-cost technologies that remove the metals from water but also result in toxic by-products [1]. Adsorption has been identified as a low-cost, convenient, and highly effective method for heavy metal control, even when metals are present in trace levels [9,10]. The key approach to adsorption technology is to develop efficient, environmentally friendly, and cheap adsorbents [8]. Natural minerals such as clays [8], silicates (wollastonite) [11,12], and zeolites [13,14] are potential sorbents that exist naturally on the earth's surface. Those minerals also contain exchangeable cations making them efficient biosorbents [15].

Cordierite is a magnesium iron aluminum cyclosilicate with a nominal molecular formula of $(\text{Mg,Fe})_2\text{Al}_3(\text{Si}_5\text{AlO}_{18})$. Cordierite typically occurs in contact or regional metamorphism of pelitic rocks. Natural cordierite is non-porous and is not useful for environmental technologies. Porous cordierite-based ceramics have been widely used as filters for diesel emission and for molten metals, devices where chemical durability and permeability are required at high temperatures. Cordierite is attractive for such applications due to its low thermal expansion coefficient, which results in high resistance to thermal shock. Also, it is widely used in catalyst supports, gas distributors, selective membranes, and pollution control [16,17]. The properties of porous ceramics and efficacy in filter/membrane systems strongly depend on the morphology, size, and distribution of pores, which are directly connected to processing and fabrication steps. Several methods are known for the preparation of porous ceramics, such as polymer-sponge [18], brush-coating [19], the addition of pore-forming agents (PFA) [20,21], and sol-gel processing [22]. PFA increase the porosity and decrease the grain size of the resulting ceramics. In particular, organic PFA of biological origin can be used to control the amount, size, and shape of pores in ceramics [23]. Zivcová et al. [23] compared less common organic PFA (e.g., lycopodium, coffee, flour, semolina, and poppy seeds) to the starch, which has become a popular PFA for ceramics during the last decade.

To the best of our knowledge, no attempts have been made to either: (1) investigate the influence of cotton-derived nanocellulose (NC) or yeast (Y) isolated from the soil as PFA on microstructure or (2) study the effect of mechanical activation on the adsorption properties of cordierite-based ceramics.

In the present study, porous cordierite-based ceramics were prepared at relatively low temperatures using cordierite-based powders as a bonding phase along with Y or NC as PFA. The effect of mechanical activation and different PFA on the phase composition and microstructure was studied along with the influence of modification

conditions on adsorption performances of polyethyleneimine functionalized cordierite-based composites.

2. Experimental procedure

2.1. Materials

The following starting materials were used: MgO , Al_2O_3 , and SiO_2 powders, ethanol, toluene, ultra-pure HNO_3 , concentrated H_2SO_4 , 3-aminopropyltrimethoxysilane (APTMS), glutaraldehyde (GLA), sodium acetate, sodium chloride, and polyethylenimine (PEI). All were supplied by Sigma-Aldrich, (Germany). Single-element atomic absorption spectroscopy standard solutions of nickel(II) and cadmium(II) ions supplied by Carl Roth GmbH & Co., Germany. Deionized water (18 M Ω cm) was used in all experiments. The cotton used as the NC PFA was purchased from NIVA, Novi Sad Industry of Cotton, Serbia.

2.2. Synthesis of cordierite

SiO_2 , MgO , and Al_2O_3 powders were calcined at 1,000°C for 2 h, to decompose hydroxides or other species to oxides. Mixtures of MgO , Al_2O_3 , and SiO_2 in the 2:2:5 molar ratios were mechanically activated by grinding in a high-energy Fritsch Pulverisette, (Idar-Oberstein, Germany), planetary ball mill. ZrO_2 vessels and balls were used with a powder-to-balls mass ratio of 1:40. The milling process was performed with ethanol in the air for 10, 40, or 80 min. After milling, powders were dried, and then pressed at 300 MPa into pellets with an 8 mm radius. The pellets were sintered by heating at 20°C min⁻¹ in the air to 1,350°C for 2 h. Sintered specimens were crushed and sieved to produce “as-prepared” cordierite.

2.3. Synthesis of bio PFA

2.3.1. NC isolation

Acid hydrolysis of cotton was done according to the procedure described previously [24,25]. In a 1 L Erlenmeyer flask containing 20 g of cotton, 200 mL of 64% H_2SO_4 solution was added drop-wise keeping the temperature to no higher than ~40°C. The cotton dispersion was washed with deionized water (DIW) using repeated centrifugation ($n = 6,000$ rpm) and sonication cycles. The centrifugation step was repeated until the supernate reached a pH value of 4. The last wash was conducted using dialysis with deionized water until the wash water maintained a constant pH value of 5.5.

2.3.2. Yeast isolation

Yeast was isolated from soil (experimental field Radmilovac, Serbia) using the serial dilution method. Yeast extract-peptone-dextrose (YPD) medium, which consisted of 1 wt.% yeast extract, 2 wt.% peptone, and 2 wt.% dextrose, was used for the isolation at the temperature of 28°C for 48 h [26]. A volume of 100 mL of YPD was inoculated by the yeast isolate. Incubation was performed in an orbital shaker (Biosan-20KS, Latvia) for 2 d at 28°C and 150 rpm. The final yeast concentration in the medium was 1·10⁸ CFU mL⁻¹, which corresponds to the absorbance of 0.5 at 780 nm (T70 UV/VIS spectrometer, PG Instruments Ltd., UK).

2.4. Preparation of porous cordierite biosorbent support

The as-prepared cordierite was mixed with 20 wt.% of Y (0.1 g Y + 0.4 g cordierite per sample) or 20 wt.% NC (0.1 g NC + 0.4 g cordierite per sample). Both mixtures were pressed into pellets at approximately 500 MPa and sintered by heating at 5°C min⁻¹ to 700°C in air. The resulting sintered cordierite supports were denoted as C₀-Y, C₁₀-Y, C₄₀-Y, C₈₀-Y, C₀-NC, C₁₀-NC, C₄₀-NC, and C₈₀-NC, according to activation times and PFA.

2.5. Coating the cordierite-based supports with polyethyleneimine

Cordierite supports were coated with polyethyleneimine in a two-step process according to the procedure described elsewhere [27]. In the first step, 1.0 g of porous sintered cordierite support was dispersed in 20 mL of toluene in a dry three-necked glass reactor of 50 mL, equipped with a magnetic stirrer, reflux condenser, thermometer, a nitrogen inlet, and calcium-chloride tube. After cordierite dispersion, a 10 wt.% solution of the silane coupling agent APTMS in toluene was added dropwise and the functionalization was continued for 24 h at 25°C under nitrogen. APTMS modified supports were washed with toluene three times, re-dispersed in 20 mL of toluene, and activated by reaction with glutaraldehyde (GLA) for 8 h at 5°C (2.5 wt.% of glutaraldehyde on cordierite support mass). After the formation of APTMS–aldehyde groups obtained cordierite supports were washed with ethanol, dried at 30°C for 2 h under vacuum before the second modification step.

Cordierite-supported PEI based composites were prepared in a dry three-necked glass reactor of 50 mL, equipped with a magnetic stirrer, reflux condenser, and calcium-chloride tube. Next, 0.5 g of PEI was added to 0.5 g

of APTMS–aldehyde modified cordierite-based supports suspended in 20 mL of 100 mM bicarbonate solution with pH 10. The reaction was carried out 24 h at room temperature under continuous stirring. The glutaraldehyde groups were reduced by adding solid sodium borohydride to achieve a concentration of 10 mg mL⁻¹ and the resulting mixture was stirred for 2 h. In the end, porous cordierite-supported PEI based composites (C_n-Y-PEI and C_n-NC-PEI, n = 10, 40, or 80 min) were washed with 100 mM sodium acetate (pH 4) and 1 M sodium chloride, and finally with an excess of distilled water. The synthesized cordierite-supported PEI-based composites were used as sorbents for nickel(II) and cadmium(II) ions in aqueous solution. The modification procedure and complexation of the amine surface groups are summarized in Fig. 1.

2.6. Adsorption and kinetic experiments

Batch adsorption and kinetic experiments for Cd²⁺ and Ni²⁺ removal were conducted by mixing with laboratory shaker (Digital Heating Shaking Drybath by Thermo Scientific). Masses of C₄₀-Y-PEI and C₄₀-NC-PEI of 1.0, 2.5, 5.0, 7.5, and 10 mg were placed in vials containing 5 mL of standard solutions containing initial concentrations (C_i) of 10 mg L⁻¹ of Cd²⁺ or Ni²⁺ with pH values of 7.5. Adsorption and kinetic experiments were performed at three temperatures, 25°C, 35°C, and 45°C and contact times ranging from 5 to 90 min. The adsorption capacities were calculated using Eq. (1):

$$q = \left(\frac{C_i - C_f}{m} \right) V \quad (1)$$

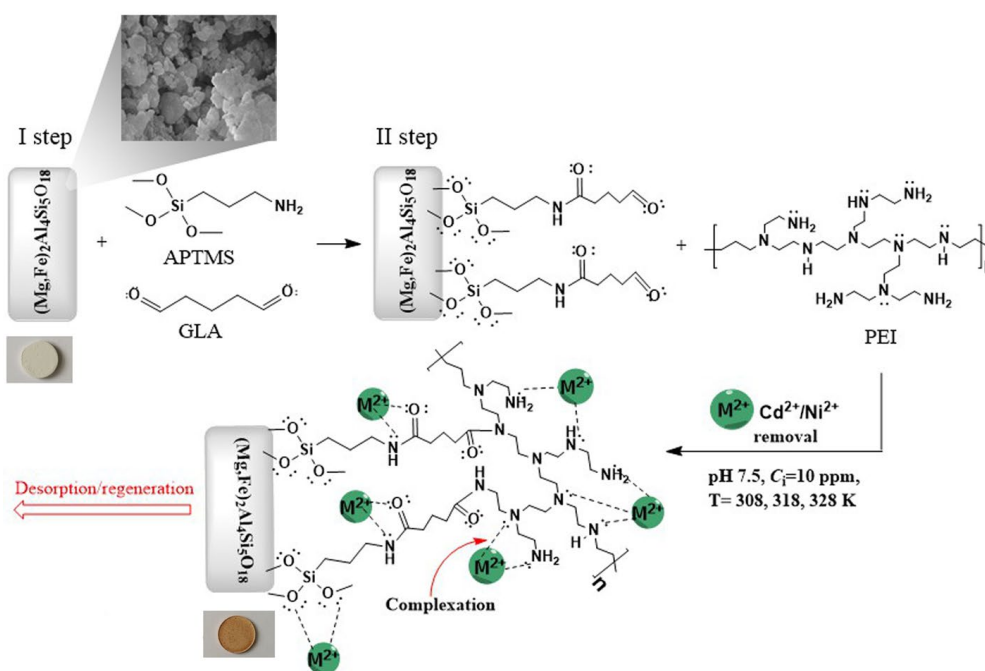


Fig. 1. Modification steps and complexation of the amine surface groups with Cd²⁺ and Ni²⁺ ions.

where q is adsorption capacity in mg g^{-1} , C_i and C_f are initial and final concentrations of Cd^{2+} or Ni^{2+} in mg L^{-1} , V is solution volume in L, and m is the mass of adsorbent in g. After adsorption, $\text{C}_{40}\text{-Y-PEI}$ and $\text{C}_{40}\text{-NC-PEI}$ adsorbents were washed with an excess of deionized water.

2.7. Characterization methods

X-ray powder diffraction (XRD) patterns were obtained using a Philips PW-1050 diffractometer, (Netherlands) with Cu-K α radiation and a step/time scan mode of 0.05°/s.

Fourier-transform infrared spectroscopy (FTIR) spectra of the cordierite-based adsorbents were recorded in absorbance mode using a Nicolet™ iS™ 10 FTIR spectrometer (Thermo Fisher Scientific, Waltham, Massachusetts, United States) with Smart iTR™ attenuated total reflectance (ATR) sampling accessories, within a range of 400–4,000 cm^{-1} , at a resolution of 4 cm^{-1} and in 20 scan modes.

Microstructural characterization of NC was performed on a transmission electron microscopy (TEM) JEM-1400, (JEOL, Japan).

The morphology of the NC, powders, and sintered specimens was analyzed by the scanning electron microscopy (SEM; JEOL JSM-6390 LV, Japan). Prior to SEM observations, the powders and crushed sintered samples were coated with gold to minimize charging.

Thermogravimetric-mass spectrometry analyses (TG-MS) were used to study the gases evolved during the heating of the samples. The experiments were performed using the TG/DSC 111 from Setaram (France), consisting of a quartz microreactor heated in a vertical furnace. Approximately 2 mg of each sample was heated from 25°C to 800°C with a heating rate of 10°C min^{-1} . The experiments were carried out in the helium (flow rate of 30 $\text{cm}^3 \text{min}^{-1}$). During heating, mass spectrometry was used to analyze the resulting gases.

The porosity of the cordierite supports after activation and cordierite-supported PEI composites were evaluated by a procedure described previously [28]. Material (skeletal) and bulk density, Q_M and Q_P were calculated from Eqs. (2) and (3):

$$Q_M = \frac{m_M}{V} - \left(\frac{m_W - m_M}{q_s} \right) \quad (2)$$

$$Q_P = \frac{m_M}{V} \quad (3)$$

where m_M is the dry weight; m_W is the weight saturated with ethanol; V is the sample volume, and q_s is the density of ethanol. The sample porosity (ε_p) was calculated from the material density and the bulk density using the Eq. (4) [28]:

$$\varepsilon_p = \frac{Q_M - Q_P}{Q_P} = 1 - \frac{Q_P}{Q_M} \quad (4)$$

Amino group (AG) content was determined according to the procedure described by Vuković et al. [29] as follows: 10 mg of $\text{C}_{40}\text{-Y-PEI}$ or $\text{C}_{40}\text{-NC-PEI}$ adsorbent was placed in 20 mL of 0.01 mol L^{-1} HCl, and ultrasonicated for 30 min. The remaining solids were removed by filtration, and

10 mL of the filtered solution was titrated with a 0.01 mol L^{-1} NaOH solution containing phenolphthalein. The aforementioned technique is based on the reaction of an unknown concentration of amino groups and with a known concentration of acid (HCl, 0.01 mol L^{-1}). The amount of excess HCl is determined with NaOH titration. Then, the amount of amino groups is determined based on the difference between the total amount of HCl used to treat the solution and the amount of HCl determined by NaOH titration [29].

The pH value of the point of zero charges, pH_{PZC} , for the amino coated C-40-Y and C-40-NC was measured by the pH drift method. The concentration of Cd^{2+} and Ni^{2+} in the solutions after adsorption and kinetic experiments were analyzed by atomic absorption spectroscopy (PinAAcle 900T, PerkinElmer, Waltham, Massachusetts, U.S.).

3. Results and discussion

3.1. NC pore-former decomposition

The cavities formed by burn-out (thermal degradation) of the pore-former during sintering act as the sites of the pore generations. The size and shape of pores/cavities depend on the microstructure of the pore-former and the number of volatile compounds produced at the sintering temperature. The NC isolated from cotton has a sponge-like porous structure with crystal lengths in the range of 90 to 200 nm and diameters of approximately 50 nm (Figs. S1b and d). The thermal degradation of NC takes place in a three-step process resulting in three observed regions on the thermogravimetric analysis (TGA) plot (Fig. S1c). At temperatures below 200°C, moisture removal occurs (region I). Reactions such as dehydration, oxidation, and decarboxylation occur at temperatures from 200°C to 300°C (region II), while trans-glycosylation occurs at higher temperatures (region III) [25]. The decomposition of NC is expected to result in open porosity in cordierite with interconnected small and large pores.

3.2. XRD analysis

The phase compositions of the non-activated and activated samples after the first sintering process, after mixing with Y as a PFA, and with additional sintering are presented in Fig. 2. Peak identification was carried out using JCPDS cards 075-1439 for cordierite, 085-1054 for SiO_2 , 089-1625 for Mg_2SiO_4 , and 083-1375 for ZrSiO_4 . The XRD pattern of the initial non-activated sintered sample ($\text{C}_0\text{-Y}$) indicated that several phases were present— $\text{Mg}_2\text{Al}_4\text{Si}_5\text{O}_{18}$, $\alpha\text{-SiO}_2$, and Mg_2SiO_4 . The formation of cordierite began during the sintering of the starting mixture, although significant amounts of the starting SiO_2 powder and spinel Mg_2SiO_4 were also present. The SiO_2 was no longer present in activated and sintered samples $\text{C}_{10}\text{-Y}$, $\text{C}_{40}\text{-Y}$, and $\text{C}_{80}\text{-Y}$, which means that mechanical activation led to better reactivity of powders. Mechanical activation led to a higher degree of reaction among the starting compound, which resulted in the increased amounts of cordierite (from 38.3 wt.% in $\text{C}_0\text{-Y}$ to 80.4 wt.% in $\text{C}_{10}\text{-Y}$, 70.5 wt.% in $\text{C}_{40}\text{-Y}$, and 77.5 wt.% in $\text{C}_{80}\text{-Y}$). The same amount of spinel phase was present in all activated samples.

The diffraction patterns of the activated and sintered samples, besides well-crystallized sharp peaks of cordierite,

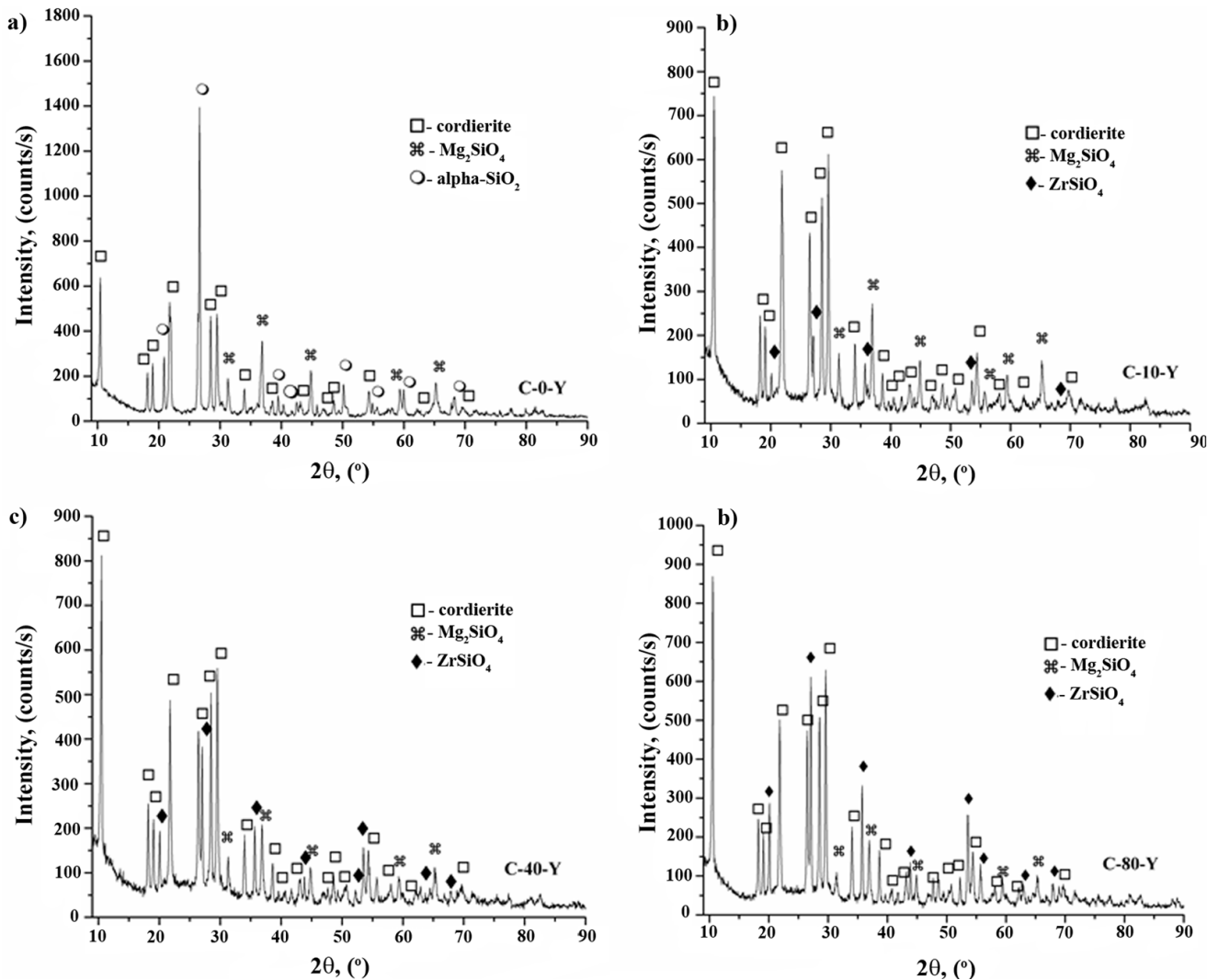


Fig. 2. XRD patterns of starting and mechanically activated and sintered cordierite samples mixed with yeast and additionally sintered.

showed small amounts of $ZrSiO_4$ (approx. 4.5 wt.% for C_{10-Y}). The amount increased with longer activation times due to contamination from the ZrO_2 jars and balls used for high-energy ball milling. The XRD patterns of cordierite samples mixed with NC as a PFA were identical to those presented in Fig. 2. Pore agents and the subsequent 700°C sintering step had no influence on phase compositions.

3.3. Morphological and textural properties

The influence of activation time and addition of bio-pore-formers on the morphological and textural properties of the cordierite support was investigated by SEM. The micrographs of the initial non-activated (NA) MgO , Al_2O_3 , and SiO_2 powders, powder mixtures activated for 10, 40, and 80 min, and after sintering on 1,350°C for 2 h are presented in Fig. 3. The initial powder consisted of large polygonal-shaped, layered particles that were more than 10 μm long, and smaller irregularly shaped particles less than 1 μm . An uneven particle size distributions were

observed. Mechanical activation of the initial MgO , Al_2O_3 , and SiO_2 powders for 10 min led to particle attrition and a more homogeneous particle size distribution compared to the NA powders (Fig. 3b). Activated particles were oval in shape. Secondary agglomeration was detected after 40 min of activation, as presented in Fig. 3c. Large agglomerates formed during activation with smaller particles around them. Prolonged mechanical activation (80 min – Fig. 3d) resulted in additional breakage of agglomerates and their attrition, although some of them remained.

After the sintering of the NA powders mixture at 1,350°C for 2 h, blocks of cordierite-based ceramics are visible in Fig. 3e. Large grain blocks over 20 μm long were a consequence of sintering the starting powder, which consisted of non-uniformly distributed, large powder particles. Sintering of activated powders led to denser microstructures where all sintered particles retained their initial shape (Figs. 3f–h). The microstructure of sintered powders for 40 and 80 min revealed two different kinds of grains: large grains that resulted from sintered

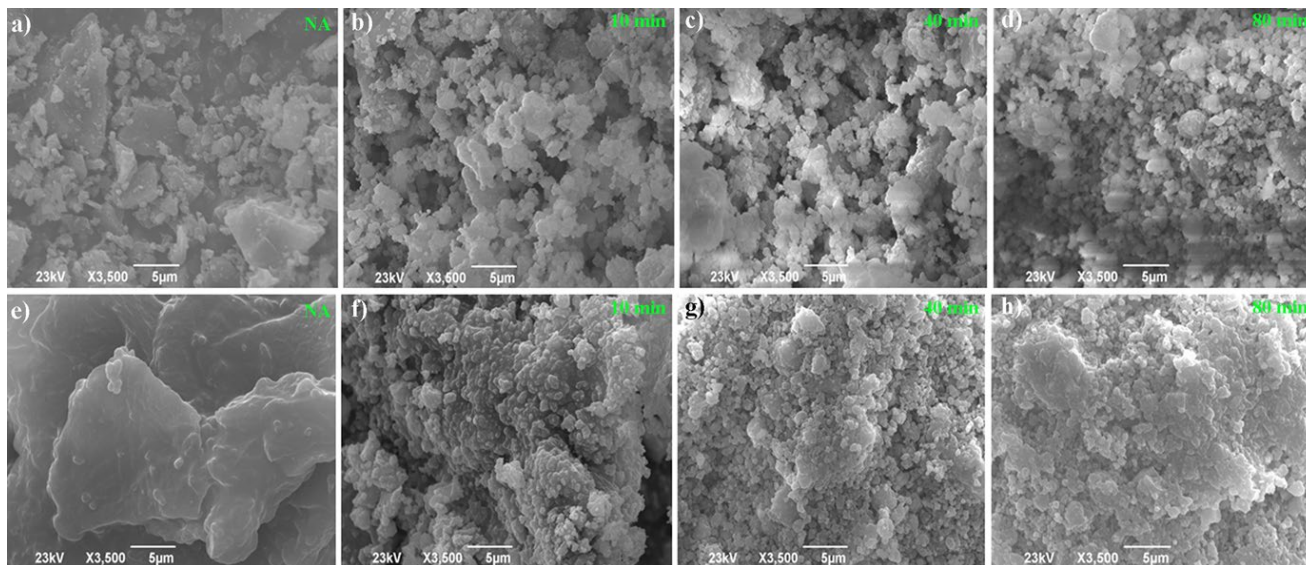


Fig. 3. SEM micrographs of (a) non-activated (NA) initial powder mixture, initial powder mixture activated, (b) 10, (c) 40, (d) 80 min; sintered (1,350°C for 2 h), (e) NA powder mixture, initial powder mixture activated, (f) 10, (g) 40, and (h) 80 min.

agglomerates and smaller grains that resulted from small mixed powder particles. It can be concluded that the microstructures of sintered powders activated for 10, 40, or 80 min were very similar.

Micrographs of as-sintered cordierite mixed with PFA, Y, or NC, and additionally sintered at 700°C to transform the PFA into gaseous products are presented in Fig. 4. Open pores are noticed in both cases, except for differently shaped grains. A sample that used yeast as the PFA possessed agglomerates, which consisted of both smaller and larger grains (Figs. 4b–d). A more uniform grain size distribution was present in the sample that used NC as the PFA. Yeast is composed of proteins (amino/nucleic acid, ≈47 wt.%), carbohydrates (≈33 wt.%), and fats and/or other minerals (≈10 wt.%) which produce lower amounts of volatile products during the sintering [30], which led to the formation of smaller grains after sintering. NC has a high molecular weight combined with a linear homopolymer consisting of repeating β-D-anhydroglucopyranose units linked together by β-1,4-glycosidic bonds in both crystalline and amorphous regions, its thermal degradation products are more uniform in composition, which led to the formation of polygonal grains [31]. During the sintering process, the thermal degradation of NC took place in a multi-step reaction: dehydration, chain scission, oxidation, decarboxylation, and transglycosylation reactions, which were followed by releasing of lower amounts of volatile compounds [25].

Increasing activation time caused a decrease in pore size. Grains were smaller within the cordierite samples activated for 40 and 80 min with either Y or NC as the PFA (Figs. 3c, d, g, and h). Open porosity was noticed and the pores were connected in the samples activated for 40 min. The microstructure of the cordierite samples activated for 80 min with Y or NC PFAs in Fig. 3d and h possessed more honeycomb-like grains. The grains consisted of small sintered particles that were interconnected by necks between

them, with porosity that was not interconnected. The porosity determination results of the initial non-activated and activated cordierite support with Y and NC PFAs after sintering are presented in Table 1.

Activation (Fig. 3) leads to a variation in the amount of porosity in the cordierite-supported polyethylenimine composites [32]. Sample porosity increased with the increasing activation time up to 40 min, after which porosity decreased. Higher porosity was obtained for the samples with NC as the PFA. However, the microstructures obtained for C₄₀-NC and C₄₀-Y indicated uniform grain distribution, which is why those specimens were used in subsequent adsorption experiments.

3.4. ATR-FTIR analysis

FTIR analysis (Fig. 5) revealed that bare cordierite supports (C₄₀-NC) had bands typical of silica at 769 cm⁻¹ (Si–O–Si) and 953 cm⁻¹ (Si–O–Si). The bands observed at 695 and 679 cm⁻¹ are commonly assigned to Mg–O bonds and those at 909 and 954 cm⁻¹ signify Mg–O–Si vibrations [33]. The low-intensity broadband present between 3,200 and 3,500 cm⁻¹ observed for the bare cordierite support (C₄₀-NC) is due to the presence of molecular water. Weak absorption bands at around 2,815–2,934 cm⁻¹ can be attributed to organic carbon stretching vibration mode [34]. The intensity of those bands increased with PEI modification of cordierite. Moreover, the presence of PEI moieties in various C₄₀-NC-PEI samples was apparent by the intensity of the bending mode from 1,625 to 1,650 cm⁻¹. Lower intensity bands from 1,000–1,250 cm⁻¹ and 679–909 cm⁻¹ originated from C–N, and NH₂/N–H vibrations, respectively. The absence of band around 1,720 cm⁻¹ from the C=O stretching vibration of GLA confirmed good coverage of C₄₀-NC coverage by PEI as the underlying APTMS silane and GLA coating were not visible after reaction with PEI [35]. The presence of amino groups was confirmed by the determination

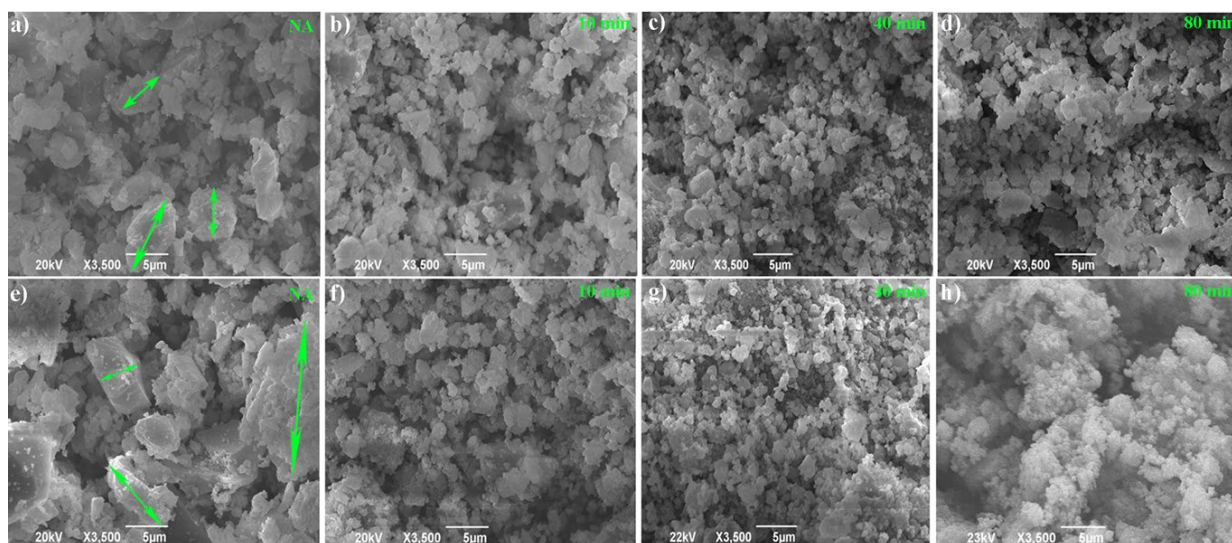


Fig. 4. SEM micrographs of (a) NA sintered initial powder mixture with yeast (700°C), sintered initial powder mixture with yeast previously activated, (b) 10, (c) 40, (d) 80 min; (e) NA sintered initial powder mixture with NC (700°C), sintered initial powder mixture with NC previously activated, (f) 10, (g) 40, and (h) 80 min.

Table 1

Porosity determination results of the initial non-activated and activated cordierite supports with Y and NC bio pore-forming agents after sintering

	Y bio pore-forming agent			
	C-Y	C ₁₀ -Y	C ₄₀ -Y	C ₈₀ -Y
ϵ_p , %	25	45	68	47
	NC bio pore-forming agent			
	C-NC	C ₁₀ -NC	C ₄₀ -NC	C ₈₀ -NC
ϵ_p , %	22	57	70	56

of AG content and a slightly higher number of the amino group was observed for C₄₀-NC-PEI (3.2 mmol g⁻¹). For C₄₀-Y-PEI, the number of amino groups was 3.0 mmol g⁻¹.

3.5. Point of zero charges (pH_{PZC}) determination

Adsorbent surface properties, morphology/texture, and adsorption conditions (acid/base) affect adsorbent efficiency [36]. The pH influences the speciation of dissolved materials and protonation or deprotonation of the adsorbent surface functional groups. In aqueous solution, C₄₀-Y-PEI and C₄₀-NC-PEI surfaces are covered with amino (–NH₂) groups that can be protonated in acid condition producing –NH₃⁺ ions or deprotonated in base conditions producing –NH⁻ ions [36]. The C₄₀-Y-PEI or C₄₀-NC-PEI pH_{PZC} values represent the pH value at which the surface concentrations of –NH₃⁺ and –NH⁻ groups are equal. Particularly, depending on the pH value of the prepared ionic/oxy-anionic solution, three possible paths for complexation with reactive surface groups (amino group, –NH₃⁺, or –NH⁻) are possible. Electrostatic forces between positively charged Ni²⁺ and Cd²⁺ ions and negative charges

of –NH⁻ are responsible for adsorption [37,38]. The measured pH_{PZC} of both C₄₀-Y-PEI and C₄₀-NC-PEI was 7.2 (Fig. S2a). From the speciation diagram of Cd²⁺ and Ni²⁺ (Figs. S2b and c), obtained using MINTEQ. 3.0 software [39], high removal efficiencies would be expected in the pH region 7–8 for both Cd²⁺ and Ni²⁺, while adsorption capabilities at pH > 8 could be enhanced by precipitation of insoluble metal hydroxides [40]. Thus, adsorption curves for Cd²⁺ and Ni²⁺ represent the only adsorption with excluded precipitation at pH > 8. According to the speciation predictions for pH < 8, removal of Cd²⁺ and Ni²⁺ was not affected by hydroxide/salt precipitation, meaning that concentration changes were related to adsorption by the composites [40]. In this sense, the selection of pH 7.5 for Cd²⁺ and Ni²⁺ removal was a logical choice to achieve high adsorption capacities.

3.6. Adsorption and kinetic study

The Langmuir 1 isotherm model is given by Eq. (5), while adsorption thermodynamic parameters are estimated using the Gibbs free energy, Eq. (6), and the linearized van't Hoff Eq. (7) (van't Hoff plot) as follows [1,41]:

$$q_e = \frac{(Kq_{\max}C_e)}{(1 + KC_e)} \quad (5)$$

$$\Delta G^\circ = -RT \ln K_L \quad (6)$$

$$\ln K_L = -\frac{\Delta H^\circ}{RT} + \frac{\Delta S^\circ}{R} \quad (7)$$

where C_e is the equilibrium concentration of ions in mol L⁻¹, q_e is the amount of adsorbed ions per weight of C₄₀-Y-PEI and C₄₀-NC-PEI adsorbents at equilibrium in mol g⁻¹,

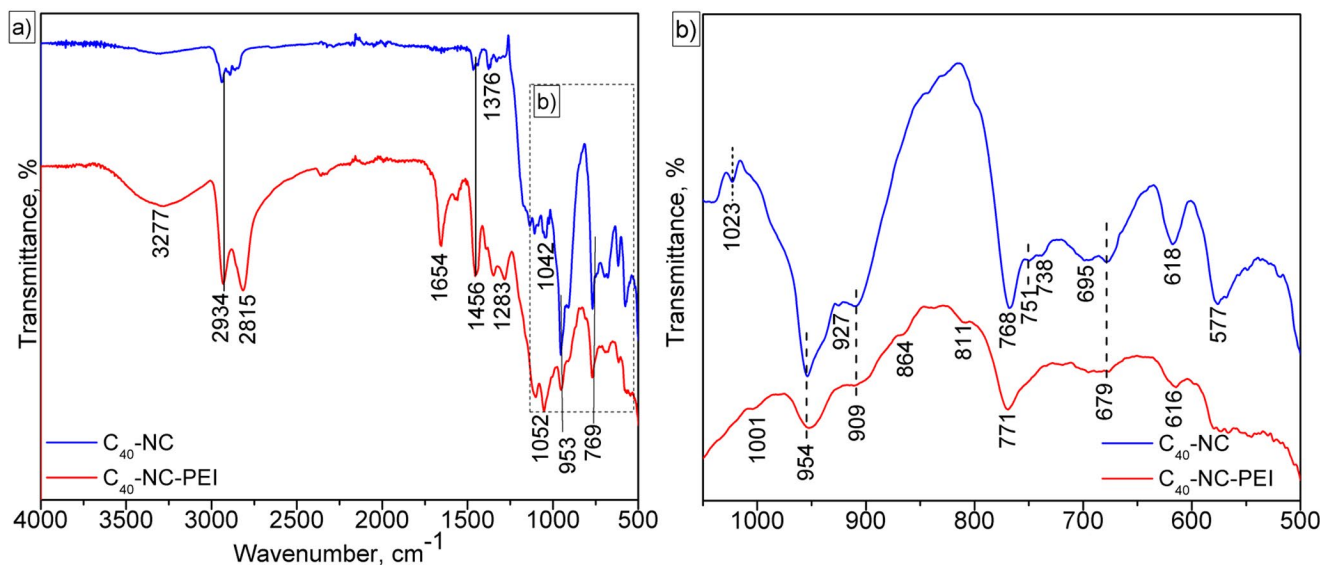


Fig. 5. ATR-FTIR spectra of the (a) C_{40} -NC and (b) C_{40} -NC-PEI.

K and K_L are Langmuir constants related to sorption affinity in $L\ mg^{-1}$ and $L\ mol^{-1}$, respectively, and q_{max} is the maximum sorption capacity in $mol\ g^{-1}$. In thermodynamic equations, ΔG° is the change of standard state Gibbs free energy in $kJ\ mol^{-1}$, ΔH° is the change of standard enthalpy in $kJ\ mol^{-1}$, ΔS° is the change of standard entropy in $kJ\ mol^{-1}$, T is the absolute temperature in K, and R is the ideal gas constant ($0.008314\ kJ\ mol^{-1}\ K^{-1}$). The values of Langmuir 1 adsorption isotherm and thermodynamic parameters at 25°C, 35°C, and 45°C for Cd^{2+} and Ni^{2+} ions are presented in Table 2, which show an increase in adsorption capacity and Langmuir 1 constants with increasing temperature. The Langmuir model assumed monolayer adsorption with equal enthalpy and energy for all reactive sites. According to the Langmuir isotherm, the energy of adsorption is generally considerably larger than for the second or higher layers, which makes multilayer adsorption less likely [42]. Higher q_e values are obtained for samples with NC PFA at all investigated temperatures due to the higher amount of porosity that consisted of open, interconnected pores (Table 2). Langmuir 1 adsorption isotherm plots are shown in Fig. S3.

The ΔG° values were negative for both metals and ranged from -46.24 to $-41.20\ kJ\ mol^{-1}$. The values indicate that adsorption occurs via spontaneous reactions involving both physisorption and chemisorption mechanisms [1,9,29,43]. The decrease of ΔG° values with increasing temperature indicates desolvation and diffusion are more likely at higher temperatures [1]. The positive ΔH° values confirm the endothermic nature of the Cd^{2+} and Ni^{2+} adsorption (Table 2) [41]. Slightly higher ΔH° values are obtained for adsorption of Ni^{2+} and indicate a slightly higher energetic contribution of Ni^{2+}/C_{40} -Y-PEI and C_{40} -NC-PEI surface interaction, and lesser diffusion processes [1]. The positive values of ΔS° indicate an increase in randomness/disorder on boundary solid-liquid surface [1].

Time dependence of Cd^{2+} and Ni^{2+} adsorption was studied in a batch system with setting an ion concentration of $125\ mg\ L^{-1}$ and pH of 7.5 for suspensions of C_{40} -Y-PEI and

C_{40} -NC-PEI. The concentrations of the ions after adsorption were determined after 5, 10, 15, 30, 60, and 90 min. The concentrations were fit using different pseudo-second-order (PSO) kinetic rate, Eq. (8) to describe adsorption kinetics [44]. The key results of a kinetic study are presented in Table 3, utilizing the following kinetic model:

$$\frac{dq_t}{dt} = k_2(q_e - q_t)^2 \quad (8)$$

where the adsorption capacities at equilibrium and at pre-defined time t are q_e and q_t , respectively in $mg\ g^{-1}$, and k_2 constant is the PSO rate constant in $g\ mg^{-1}\ min^{-1}$.

The high values of the coefficient of determination, R^2 , indicate that the PSO kinetic model can be used for the prediction of adsorption kinetics for Cd^{2+} and Ni^{2+} on amino cordierite-based adsorbents. The kinetic parameters show that amine-modified cordierite-based adsorbents possess a high affinity for Cd^{2+} and Ni^{2+} ions. From the PSO kinetic law, the rate-limiting step is related to chemical adsorption (valence forces through sharing or the exchange of electrons between the s reactive sites of the sorbents and metal cations) [45]. The values of k_2 and q_e increased with increasing temperature, and the highest values were obtained at 45°C. These results indicated that complexation of Cd^{2+} and Ni^{2+} with reactive amine sites on C_{40} -Y-PEI and C_{40} -NC-PEI surfaces (diffusion transport) increased with increasing temperature and that samples prepared with NC PFA had higher kinetic constants at all investigated temperatures compared to the sample with Y.

3.7. Overview of adsorption capacities of mineral silicate and amino-based adsorbents

Literature data for silicate-based mineral adsorbents and Cd^{2+} and Ni^{2+} removal are provided in Table 4. Comparison of the literature data with results for C_{40} -Y-PEI and C_{40} -NC-PEI provides key information about potential applicability

Table 2

Langmuir isotherm and thermodynamic parameters for Cd²⁺ and Ni²⁺ ions obtained at 25°C, 35°C, and 45°C (298, 308, and 318 K) using C₄₀-Y-PEI and C₄₀-NC-PEI adsorbents

		Cd ²⁺				Ni ²⁺			
C ₄₀ -Y-PEI	T (K)	q _e (mg g ⁻¹)	K (L mg ⁻¹)	K _L	R ²	q _e (mg g ⁻¹)	K (L mg ⁻¹)	K _L	R ²
	298	29.049	3.741	23,342,210.8	0.97	33.627	9.043	29,458,852.7	0.996
C ₄₀ -Y-PEI	308	31.053	4.611	28,767,337.6	0.97	35.823	11.796	38,426,878.4	0.961
	318	32.565	4.750	29,636,993.9	0.96	36.079	12.017	39,143,541.0	0.996
C ₄₀ -NC-PEI	298	39.850	9.115	28,679,171.1	0.99	39.868	5.074	16,527,048.8	0.970
	308	41.698	9.407	29,598,985.5	0.99	42.431	6.319	20,583,131.2	0.964
	318	43.070	10.258	32,277,313.6	0.99	43.206	7.046	22,951,873.7	0.967
Thermodynamic parameters									
		Cd ²⁺			Ni ²⁺				
	T (K)	ΔG° (kJ mol ⁻¹)	ΔH° (kJ mol ⁻¹)	ΔS° (J mol ⁻¹ K ⁻¹)	ΔG° (kJ mol ⁻¹)	ΔH° (kJ mol ⁻¹)	ΔS° (J mol ⁻¹ K ⁻¹)		
C ₄₀ -Y-PEI	298	-42.06			-42.63				
	308	-44.00	9.49	173.11	-44.74	11.31	181.24		
	318	-45.51			-46.24				
C ₄₀ -NC-PEI	298	-42.57			-41.20				
	308	-45.50	2.95	152.67	-43.14	12.99	181.89		
	318	-45.73			-44.83				

Table 3

Kinetic parameters obtained by the use of non-linear PSO kinetic model for the Cd²⁺ and Ni²⁺ removal using C₄₀-Y-PEI and C₄₀-NC-PEI adsorbents

298 K		Cd ²⁺	Ni ²⁺
C ₄₀ -Y-PEI	k ₂ × 10 ² (g mg ⁻¹ min ⁻¹)	0.72 ± 0.02	1.11 ± 0.02
	q _e (mg g ⁻¹)	29.31 ± 0.58	33.06 ± 0.53
	R ²	0.997	0.998
C ₄₀ -NC-PEI	k ₂ × 10 ² (g mg ⁻¹ min ⁻¹)	0.94 ± 0.02	0.94 ± 0.02
	q _e (mg g ⁻¹)	38.96 ± 0.81	39.18 ± 0.38
	R ²	0.999	0.995
308 K		Cd ²⁺	Ni ²⁺
C ₄₀ -Y-PEI	k ₂ × 10 ² (g mg ⁻¹ min ⁻¹)	0.87 ± 0.01	1.12 ± 0.01
	q _e (mg g ⁻¹)	30.08 ± 0.11	34.85 ± 0.80
	R ²	0.996	0.999
C ₄₀ -NC-PEI	k ₂ × 10 ² (g mg ⁻¹ min ⁻¹)	1.03 ± 0.02	1.02 ± 0.02
	q _e (mg g ⁻¹)	40.41 ± 0.52	40.49 ± 0.52
	R ²	0.999	0.999
318 K		Cd ²⁺	Ni ²⁺
C ₄₀ -Y-PEI	k ₂ × 10 ² (g mg ⁻¹ min ⁻¹)	1.15 ± 0.01	1.79 ± 0.02
	q _e (mg g ⁻¹)	32.44 ± 0.69	50.15 ± 0.31
	R ²	0.998	0.999
C-40-NC-PEI	k ₂ × 10 ² (g mg ⁻¹ min ⁻¹)	1.27 ± 0.01	1.28 ± 0.02
	q _e (mg g ⁻¹)	41.57 ± 0.30	40.85 ± 0.39
	R ²	0.999	0.998

Table 4
Comparison of mineral silicate adsorbents for heavy metal adsorption

Adsorbent	Ion	C_p , mg L ⁻¹	q_e , mg g ⁻¹	Reference
Wollastonite (W)	Ni ²⁺	50.0	6.50	[11]
Synthetic mineral adsorbent ^a	Cd ²⁺	–	47.0	[46]
WL- γ -APS/MG ^b	Ni ²⁺	10.0	66.14	[1]
WL- γ -APS/MG	Cd ²⁺	10.0	73.15	[1]
C ₄₀ -Y-PEI	Ni ²⁺	10.0	36.08	This work
C ₄₀ -NC-PEI	Cd ²⁺	10.0	32.56	This work
C ₄₀ -Y-PEI	Ni ²⁺	10.0	43.21	This work
C ₄₀ -NC-PEI	Cd ²⁺	10.0	43.07	This work

^aSynthetic mineral adsorbent containing wollastonite, illite, gypsum, limestone, and dolomite.

^bWollastonite modified with magnetite via aminopropylsilane cross-linker.

in the adsorption process, and the advantages/weaknesses of adsorbents as well. Maximum adsorption capacities, affinity, kinetics, and operational conditions (initial concentration, pH, contact time, temperature, etc.) are important criteria for comparison. Compared to the pure, natural mineral silicate wollastonite, significantly higher maximum adsorption capacities were obtained for C40-Y-PEI and C40-NC-PEI due to higher porosity and the presence of active surface sites [11]. Synthetic mineral adsorbents such as composites containing wollastonite, illite, gypsum, limestone, and dolomite showed a slightly higher adsorption capacity 47.0 mg g⁻¹, but its synthesis process was more complex and the precursor costs were higher [46]. Similar conclusions can be observed for wollastonite modified with magnetite by an aminopropylsilane cross-linking agent (WL- γ -APS/MG) [1].

4. Conclusions

The influence of mechanical activation as a pre-sintering preparation technique on the phase development and microstructure of cordierite-based porous ceramics was studied. Activation time of 40 min in a high energy ball-mill led to the best microstructure with the smallest grains and most uniform distribution. The Langmuir adsorption isotherms, PSO kinetics, and thermodynamic analysis results confirmed that the adsorption of Cd²⁺ and Ni²⁺ on amine-functionalized cordierite-based ceramics was a spontaneous, endothermic process. Analyses also confirmed that NC was a better PFA due to its influence on adsorption performance. The adsorption capacities of C₄₀-Y-PEI exceeded 32.57 and 36.08 mg g⁻¹ for Cd²⁺ and Ni²⁺ cations at 318 K, while C₄₀-NC-PEI exhibits the highest adsorption capacity of 43.21 mg g⁻¹ for Ni²⁺ at 318 K. In addition, the higher values of the k_2 constant indicate that porous cordierite-supported PEI-based composites are excellent materials for Ni²⁺ and Cd²⁺ removal from aqueous solutions.

Acknowledgment

This investigation was supported by the Serbian Ministry of Education, Science and Technological Development of the Republic of Serbia, and it was conducted under the project Contract No. 451-03-68/2020-14/200325.

References

- [1] J.D. Rusmirović, N. Obradović, J. Perendija, A. Umičević, A. Kapidžić, B. Vlahović, V. Pavlović, A.D. Marinković, V.B. Pavlović, Controllable synthesis of Fe₃O₄-wollastonite adsorbents for efficient heavy metal ions/oxyanions removal, *Environ. Sci. Pollut. Res.*, 26 (12) (2019) 12379–12398.
- [2] S. Jodeh, M. Shawahny, G. Hanbali, D. Jodeh, O. Dagdag, Efficiency of magnetic chitosan supported on graphene for removal of perchlorate ions from wastewater, *Environ. Technol.*, (2019) 1–27. doi: 10.1080/09593330.2019.1657963.
- [3] G.B. Vieira, G. Scaratti, F.S. Rodembusch, S.M. De Amorim, M. Peterson, G.L. Puma, R. De Fátima Peralta Muniz Moreira, Tuning the photoactivity of TiO₂ nanoarchitectures doped with cerium or neodymium and application to colour removal from wastewaters, *Environ. Technol.*, (2019) 1–15. doi:10.1080/09593330.2019.1651402.
- [4] D. Paul, Research on heavy metal pollution of river Ganga: a review, *Ann. Agrar. Sci.*, 15 (2017) 278–286.
- [5] F. Esposito, V. Memoli, G. Di Natale, M. Trifuoggi, G. Maisto, *Quercus ilex* L. leaves as filters of air Cd, Cr, Cu, Ni and Pb, *Chemosphere*, 218 (2019) 340–346.
- [6] K. Taleb, J. Markovski, Z. Veličković, J. Rusmirović, M. Rančić, V. Pavlović, A. Marinković, Arsenic removal by magnetite-loaded amino modified nano/microcellulose adsorbents: effect of functionalization and media size, *Arabian J. Chem.*, 12 (2019) 4675–4693.
- [7] US EPA, Water Quality Standards, United States Environmental Protection Agency, William Jefferson Clinton Federal Building, Washington, D.C., U.S., 2014.
- [8] S.Q. Gu, X.N. Kang, L. Wang, E. Lichtfouse, C.Y. Wang, Clay mineral adsorbents for heavy metal removal from wastewater: a review, *Environ. Chem. Lett.*, 17 (2019) 629–654.
- [10] D. Budimirović, Z.S. Veličković, V.R. Djokić, M. Milosavljević, J. Markovski, S. Lević, A.D. Marinković, Efficient As(V) removal by α -FeOOH and α -FeOOH/ α -MnO₂ embedded PEG-6-arm functionalized multiwall carbon nanotubes, *Chem. Eng. Res. Des.*, 119 (2017) 75–86.
- [11] K. Taleb, J. Markovski, M. Milosavljević, M. Marinović-Cincović, J. Rusmirović, M. Ristić, A. Marinković, Efficient arsenic removal by cross-linked macroporous polymer impregnated with hydrous iron oxide: material performance, *Chem. Eng. J.*, 279 (2015) 66–78.
- [12] Y.C. Sharma, G.S. Gupta, G. Prasad, D.C. Rupainwar, Use of wollastonite in the removal of Ni(II) from aqueous solutions, *Water Air Soil Pollut.*, 49 (1990) 69–79.
- [13] N. Obradović, S. Filipović, S. Marković, M. Mitrić, J. Rusmirović, A. Marinković, V. Antić, V. Pavlović, Influence of different pore-forming agents on wollastonite microstructures and adsorption capacities, *Ceram. Int.*, 43 (2017) 7461–7468.
- [14] Z.H. Li, J.-S. Jean, W.-T. Jiang, P.-H. Chang, C.-J. Chen, L.B. Liao, Removal of arsenic from water using Fe-exchanged natural zeolite, *J. Hazard. Mater.*, 187 (2011) 318–323.

- [15] E. Erdem, N. Karapinar, R. Donat, The removal of heavy metal cations by natural zeolites, *J. Colloid Interface Sci.*, 280 (2004) 309–314.
- [16] Y. Li, H.Z. Zhao, Effect of reduced Al_2O_3 mole ratio on fabrication of cordierite ceramic by solid-state sintering method, *Sci. Sintering*, 51 (2019) 189–197.
- [17] A. Benhammou, Y. El Hafiane, A. Abourriche, Y. Abouliatim, L. Nibou, A. Yaacoubi, N. Tessier-Doyen, A. Smith, B. Tanouti, Effects of oil shale addition and sintering cycle on the microstructure and mechanical properties of porous cordierite-ceramic, *Ceram. Int.*, 40 (2014) 8937–8944.
- [18] T.D. Senguttuvan, H.S. Kalsi, S.K. Sharda, B.K. Das, Sintering behavior of alumina rich cordierite porous ceramics, *Mater. Chem. Phys.*, 67 (2001) 146–150.
- [19] X. Wu, Z.-h. Chen, Y.-l. Feng, X.-p. Liu, X.-l. Li, Fabrication of micro-honeycomb ceramics by cloth fabric pore-forming, *Trans. Nonferrous Met. Soc. China*, 21 (2011) 2665–2670.
- [20] S.F. Liu, Y.-P. Zeng, D.L. Jiang, Fabrication and characterization of cordierite-bonded porous SiC ceramics, *Ceram. Int.*, 35 (2009) 597–602.
- [21] N. Obradović, S. Filipović, J. Rusmirović, G. Postole, A. Marinković, D. Radić, V. Rakić, V. Pavlović, A. Auroux, Formation of porous wollastonite-based ceramics after sintering with yeast as the pore-forming agent, *Sci. Sintering*, 49 (2017) 235–246.
- [22] E.F. Krivoschapkina, P.V. Krivoschapkin, A.A. Vedyagin, Synthesis of Al_2O_3 - SiO_2 -MgO ceramics with hierarchical porous structure, *J. Adv. Ceram.*, 6 (2017) 11–19.
- [23] Z. Zivcová, E. Gregorová, W. Pabst, Alumina ceramics prepared with new pore-forming agents, *Process. Appl. Ceram.*, 2 (2008) 1–8.
- [24] J.D. Rusmirović, M.P. Rančić, V.B. Pavlović, V.M. Rakić, S. Stevanović, J. Djonlagić, A.D. Marinković, Cross-linkable modified nanocellulose/polyester resin-based composites: effect of unsaturated fatty acid nanocellulose modification on material performances, *Macromol. Mater. Eng.*, 303 (2018) 1–12.
- [25] J.D. Rusmirović, J.Z. Ivanović, V.B. Pavlović, V.M. Rakić, M.P. Rančić, V. Djokić, A.D. Marinković, Novel modified nanocellulose applicable as reinforcement in high-performance nanocomposites, *Carbohydr. Polym.*, 164 (2017) 64–74.
- [26] E. Slávková, R. Vadkertiová, The diversity of yeasts in the agricultural soil, *J. Basic Microbiol.*, 43 (2003) 430–436.
- [27] C. Mateo, O. Abian, R. Fernandez-Lafuente, J.M. Guisan, Reversible enzyme immobilization via a very strong and nondistorting ionic adsorption on support – polyethylenimine composites, *Biotechnol. Bioeng.*, 68 (2000) 98–105.
- [28] H. Sontheimer, J.C. Crittenden, R.S. Summers, Activated Carbon for Water Treatment, DVGW-Forschungsstelle, Engler-Bunte-Institut, Universität Karlsruhe (TH), Karlsruhe, Germany, 1988, pp. 66–67.
- [29] G.D. Vuković, A.D. Marinković, S.D. Škapin, M.Đ. Ristić, R. Aleksić, A. Perić-Grujić, P.S. Uskoković, Removal of lead from water by amino modified multi-walled carbon nanotubes, *Chem. Eng. J.*, 173 (2011) 855–865.
- [30] A. Omar, R. Al-Obeed, M. Ahmed, Effect of foliar spraying with potassium dehydrogenase phosphate and yeast extract on yield and fruit quality of Sukary date palm (*Phoenix dactylifera* L.) in Saudi Arabia, *Adv. Agric. Sci.*, 6 (2018) 25–32.
- [31] J.D. Rusmirović, M.P. Rančić, A.D. Marinković, Chapter 8 – Processing and Characterization of Modified Nanocellulose/Polyester Composites, T. Stevanovic, Eds., Chemistry of Lignocellulosics: Current Trends, Taylor & Francis Group, CRC Press, Cleveland, Ohio, United States, 2018, pp. 167–213.
- [32] V. Usoltsev, S. Tikhov, A. Salanov, V. Sadykov, G. Golubkova, O. Lomovskii, Properties of porous $FeAlOy/FeAlx$ ceramic matrix composite influenced by mechanical activation of FeAl powder, *Bull. Mater. Sci.*, 36 (2013) 1195–1200.
- [33] S.Y. Ni, L. Chou, J. Chang, Preparation and characterization of forsterite (Mg_2SiO_4) bioceramics, *Ceram. Int.*, 33 (2007) 83–88.
- [34] A.S. Majumdar, G. Mathew, Raman-Infrared (IR) spectroscopy study of natural cordierites from Kalahandi, Odisha, *J. Geol. Soc. India.*, 86 (2015) 80–92.
- [35] K.M. de Lathouder, D.T.J. van Benthem, S.A. Wallin, C. Mateo, R.F. Lafuente, J.M. Guisan, F. Kapteijn, J.A. Moulijn, Polyethylenimine (PEI) functionalized ceramic monoliths as enzyme carriers: preparation and performance, *J. Mol. Catal. B: Enzym.*, 50 (2008) 20–27.
- [36] A. Popovic, J. Rusmirović, S. Levic, A. Bozic, T. Kovacevic, Amino-Functionalized Lignin Microspheres: Synthesis and Characterization of High-Performance Adsorbent for Effective Nickel(II) Ion Removal, 31st International congress on Process Industry, Belgrade, Serbia, 2018, pp. 235–239.
- [37] M.A. Ahmed, S.M. Ali, S.I. El-Dek, A. Galal, Magnetite-hematite nanoparticles prepared by green methods for heavy metal ions removal from water, *Mater. Sci. Eng., B*, 178 (2013) 744–751.
- [38] S. Rajput, C.U. Pittman Jr., D. Mohan, Magnetic magnetite (Fe_3O_4) nanoparticle synthesis and applications for lead (Pb^{2+}) and chromium (Cr^{6+}) removal from water, *J. Colloid Interface Sci.*, 468 (2016) 334–346.
- [39] J.P. Gustafsson, Visual MINTEQ. 3.0, Beta, 2011.
- [40] A. Drah, N.Z. Tomić, Z. Veličić, A.D. Marinković, Ž. Radovanović, Z. Veličković, R. Jančić-Heinemann, Highly ordered macroporous γ -alumina prepared by a modified sol-gel method with a PMMA microsphere template for enhanced Pb^{2+} , Ni^{2+} and Cd^{2+} removal, *Ceram. Int.*, 43 (2017) 13817–13827.
- [41] C.-H. Liu, Y.-H. Chuang, T.-Y. Chen, Y. Tian, H. Li, M.-K. Wang, W. Zhang, Mechanism of arsenic adsorption on magnetite nanoparticles from water: thermodynamic and spectroscopic studies, *Environ. Sci. Technol.*, 49 (2015) 7726–7734.
- [42] F. Rouquerol, J. Rouquerol, S. Kenneth, Adsorption by Powders and Porous Solids: Principles, Methodology and Application, Academic Press, USA, 1999.
- [43] Z. Veličković, G.D. Vuković, A.D. Marinković, M.S. Moldovan, A.A. Perić-Grujić, P.S. Uskoković, M.D. Ristić, Adsorption of arsenate on iron(III) oxide coated ethylenediamine functionalized multiwall carbon nanotubes, *Chem. Eng. J.*, 181–182 (2012) 174–181.
- [44] O. Bizerea Spiridon, L. Pitulice, Response to “Using of ‘pseudo-second-order model’ in adsorption”, comment letter on “Phenol removal from wastewater by adsorption on zeolitic composite” [Bizerea Spiridon et al., *Environ Sci Pollut Res* (2013) 20:6367–6381], *Environ. Sci. Pollut. Res.*, 21 (2014) 7236–7237.
- [45] H. Qiu, L. Lv, B.-c. Pan, Q.-j. Zhang, W.-m. Zhang, Q.-x. Zhang, Critical review in adsorption kinetic models, *J. Zhejiang Univ. Sci. A.*, 10 (2009) 716–724.
- [46] G. Chen, K.J. Shah, L. Shi, P.-C. Chiang, Removal of Cd(II) and Pb(II) ions from aqueous solutions by synthetic mineral adsorbent: performance and mechanisms, *Appl. Surf. Sci.*, 409 (2017) 296–305.

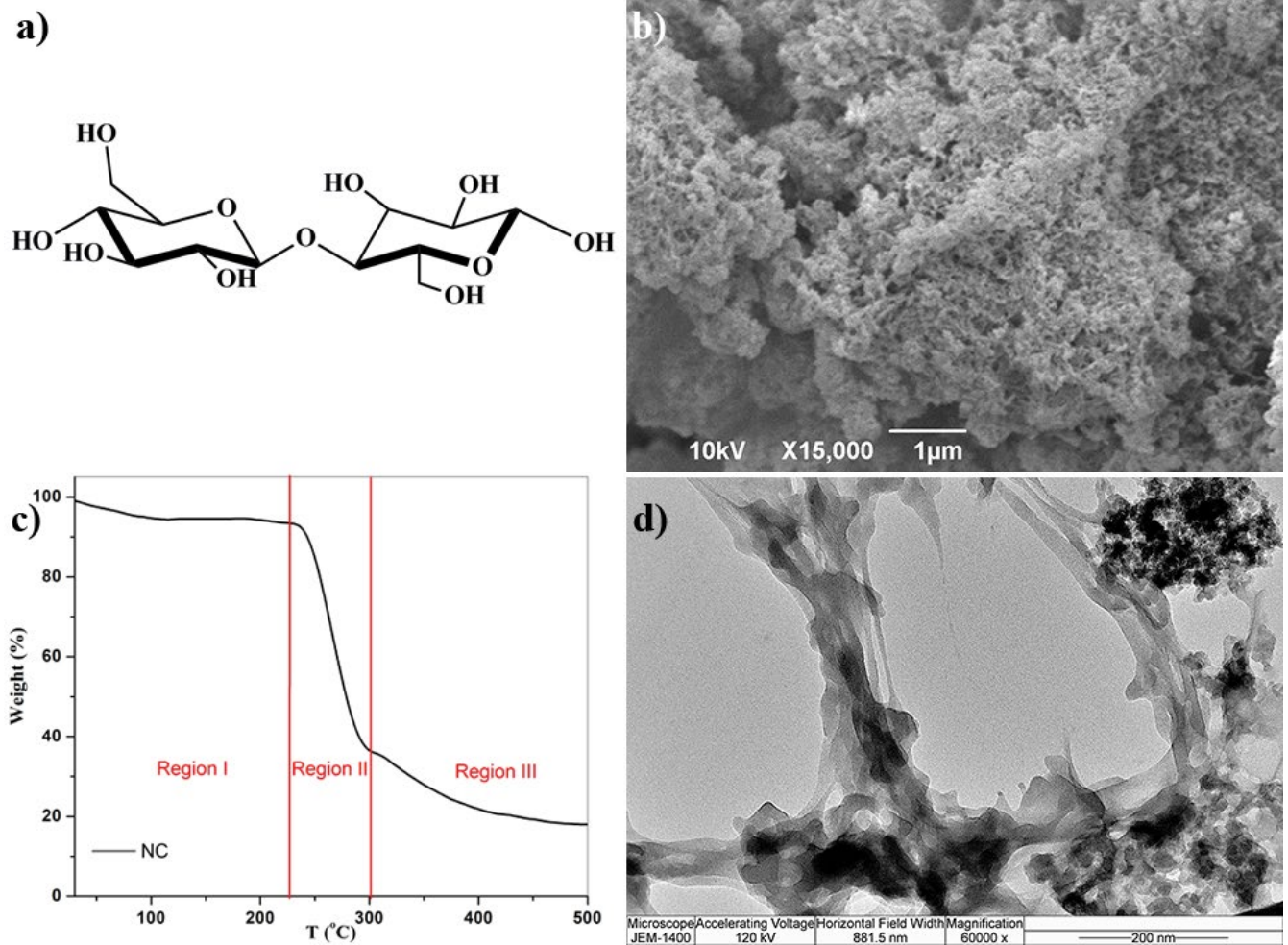
Supplementary information*S1.1. NC pore-former characterization*

Fig. S1. (a) The structural formula of the NC unit, (b) SEM micrograph of the isolated NC bio pore-forming agent, (c) TGA curve of the NC, and (d) TEM micrograph of the NC.

S1.2. Point of zero charge (pH_{PZC}) determination

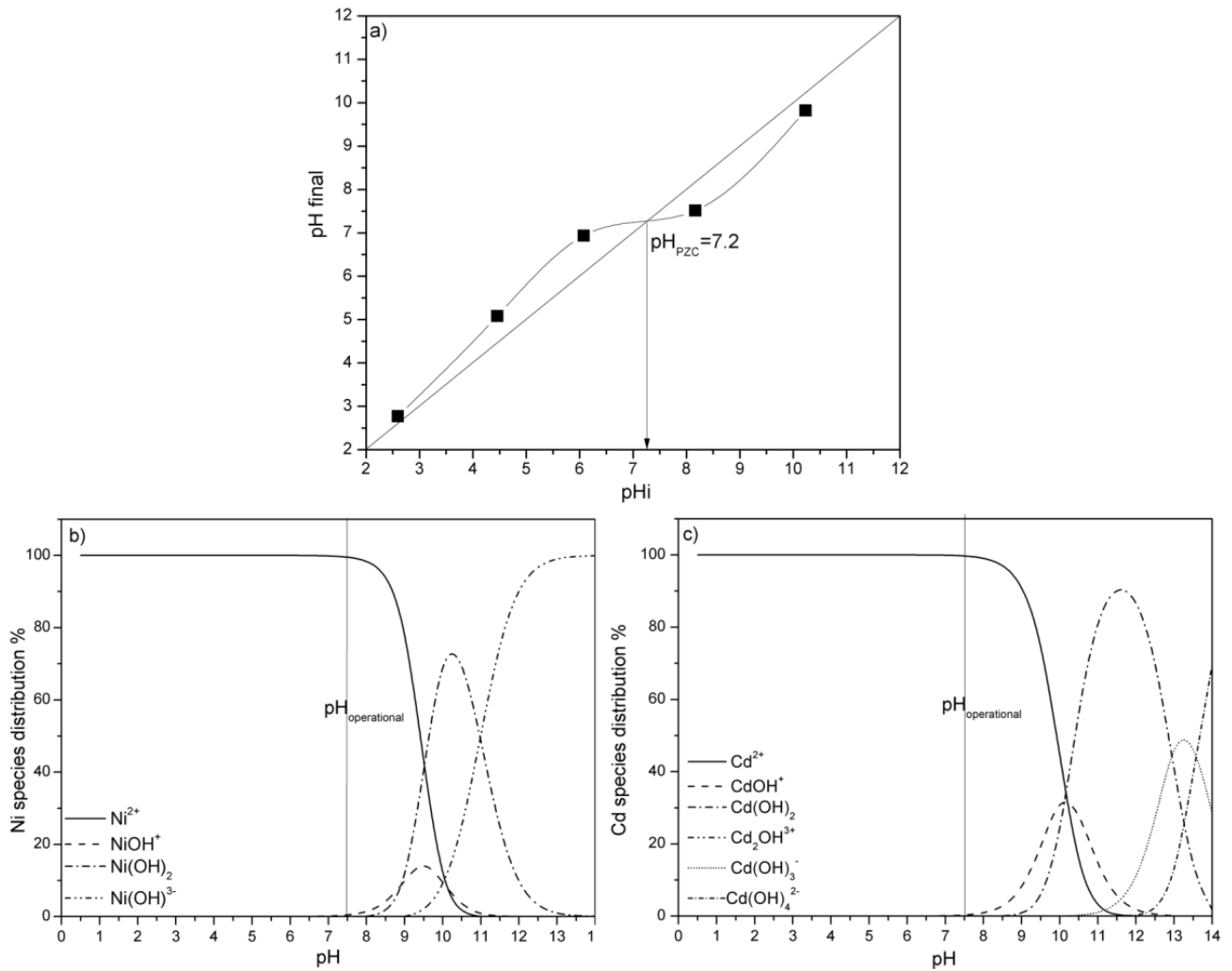


Fig. S2. Diagrams for determination of (a) pH_{PZC} , (b) Ni, and (c) Cd species distribution.

S1.3. Adsorption and kinetic study

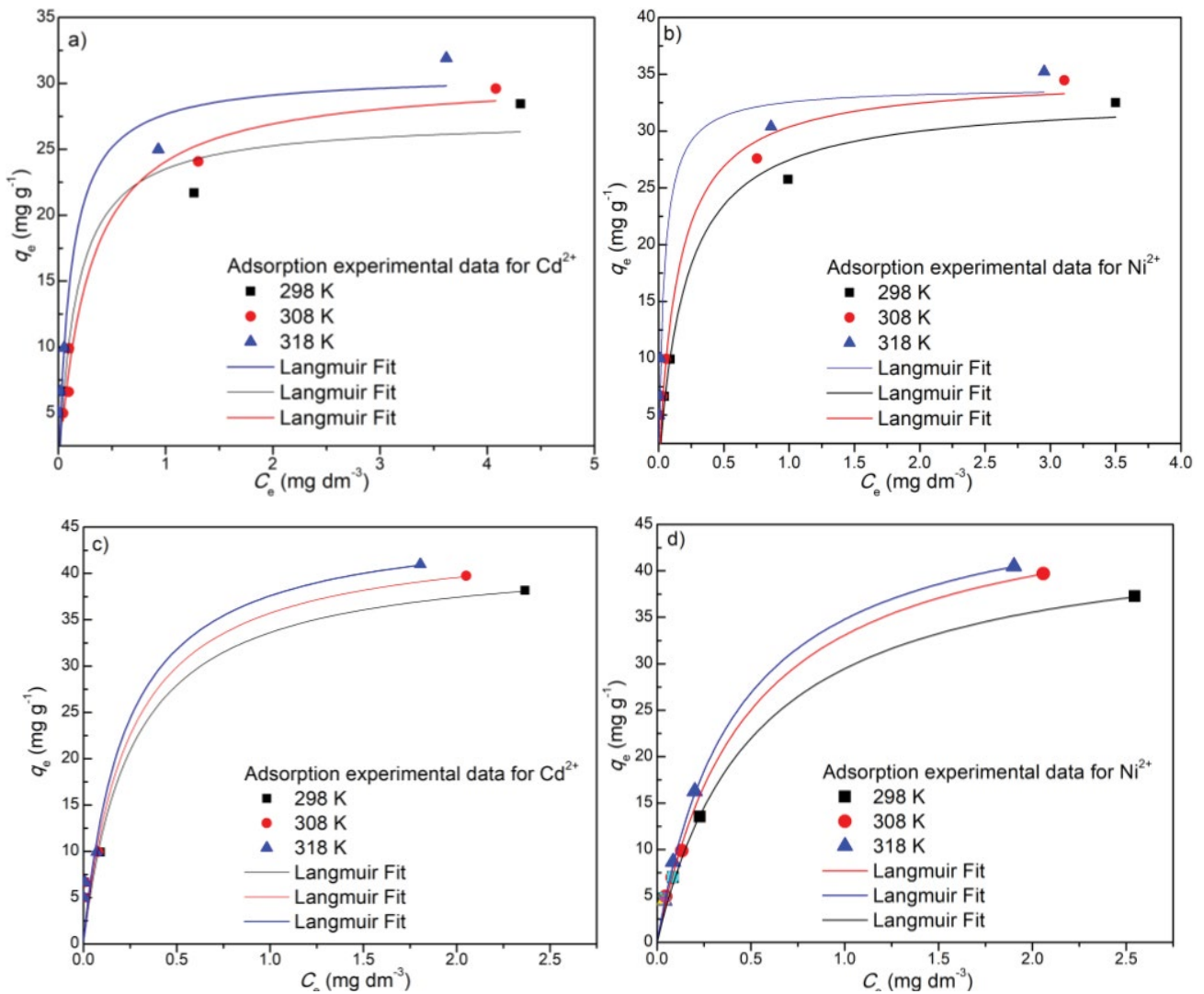


Fig. S3. Langmuir 1 adsorption isotherm plots of (a) C_{40} -Y-PEI for Cd^{2+} , (b) C_{40} -Y-PEI for Ni^{2+} , (c) C_{40} -NC-PEI for Cd^{2+} , and (d) C_{40} -NC-PEI for Ni^{2+} .